D10

DESIGN OF A FLIGHT QUALIFIED LONG-LIFE CRYOCOOLER

L. Knox, P. Patt, R. Maresca

Philips Laboratories
A Division of North American Philips Corporation
Briarcliff Manor, NY 10510

This paper describes a second generation Stirling cycle cryogenic refrigerator with a linear drive, magnetic bearings, and clearance seals, designed to produce 5 watts of cooling at 65 Kelvin and to meet Space Shuttle mission requirements. The first generation refrigerator (Engineering Model) met all performance specifications, and has operated with no failure for over 12,000 hours. It was not, however, intended to meet launch requirements. Meeting those requirements necessitated improvements in the electromagnetic bearings, the radial position sensors, and in the structural design of the moving elements. As in the first generation refrigerator, organic contamination has been eliminated by the use of all metal and ceramic construction. Reductions in system input power have also been attained by an integral magnetic spring/motor for the displacer and by more efficient linear motors and drive electronics. At the design point, the refrigerator consumes 140 watts, delivered by the system electronics.

Ferrite variable reluctance position sensors reduce the temperature drift of the magnetic bearing system. Additional bearing improvements are realized through increases in gas film damping, ac/dc force capabilities, and structural resonant frequencies. All clearance seal surfaces are specially treated to eliminate potential damage due to contact during launch and system failures. Transmitted vibrations are minimized by a six-degree-of-freedom spring mount.

The work summarized in the paper is being supported by the NASA-Goddard Space Flight Center. (Contract Number NAS5-26668)

Key words: Clearance seal; cryogenics; ferrite sensors; gas film damping; launch vibrations; linear motor; magnetic bearings; magnetic spring; Stirling cycle.

1. Introduction

A long-life refrigerator capable of providing 5 watts of cooling at 65 Kelvin has been successfully designed, fabricated, and tested by Philips Laboratories.[1] Long life was achieved by eliminating wear and working gas contamination. Wear was prevented by use of magnetic bearings and clearance seals. The working gas volume is hermetically sealed from all organic materials used in the construction which prevents degradation due to outgassing. The details of this refrigerator are described in earlier papers; parametric and life test results are presented in a companion paper[2].

A refrigerator of this type is expected to be part of a complete satellite structure which will be launched into space on the Space Shuttle. However, the ability to survive launch

vibrations was not considered in the first generation 'proof of concept' design. Analysis of the expected launch vibrations indicated that the first generation magnetic suspension system could not be modified to accommodate those produced by the shuttle. The second generation design considers these vibrations and is capable of suspending all moving elements during launch and normal operation.

This paper describes the vibration analyses performed and the design revisions which were made to accommodate the vibrations. Several cooler component improvements are also described in this paper.

2. System description

The second generation refrigerator, the Flight Prototype described here, is a single stage, moving regenerator Stirling refrigerator. The piston and displacer/regenerator are linearly reciprocated within a cylindrical housing and radially supported with active magnetic bearings. A brief overview of system construction and operation is presented in this section. A detailed description of the theory of operation of this cooler is available in earlier reports.

The cooler is comprised of a compressor and an expander section (fig. 1). The expander section contains the moving displacer/regenerator and the cold and warm side heat exchangers. The compressor section contains the compressor piston, piston linear motor and gas buffer volume. The piston and displacer are supported by the magnetic bearings, three of which also form clearance seals. Two seals direct the gas flow in the expander section during the cycle; the third seals the compression volume above the piston.

Gas at the cold end expands (i.e. cools) as the piston retracts and increases the total gas working volume. The expanding gas cools the aluminum slit cold end heat exchanger. The heat load is cooled by a thermally conductive cable (not shown) attached to the cold end heat exchanger. The cable minimizes the transmitted mechanical vibrations. The heat exchanger is stationary and supported with a long thin walled tube, or cold finger. In the next phase of the cycle, the displacer moves toward the cold end. The clearance seal forces the gas through the regenerator where it is warmed. As the piston moves toward the cold end, the heat of compression is rejected through another slit heat exchanger in the expander section housing. Finally, the displacer moves toward the compressor end cooling the gas as it flows through the regenerator thus completing the cycle. These discrete motions are approximated by continuous sinusoids, where a phase angle describes the relative timing between the displacer and compressor motion.

The piston (compressor) is reciprocated with a moving magnet linear motor, similar to that used in the Engineering Model. The current to the motor, and therefore the piston motion, is controlled with a low frequency, high efficiency pulse-width-modulated current driver system. The displacer is reciprocated with a novel integrated magnetic spring/linear motor. The phasing is controlled via the system electronics. The displacer spring/motor and the pulse-width-modulated piston motor drive system is described in more detail in a latter section of this paper.

Primary design parameters (such as piston and displacer diameter, strokes, frequency, and radial clearance to the stationary walls) were determined by considering the overall system dynamics. Trade-offs result among system dynamics, thermodynamic losses (primarily conduction), and difficulty of construction (such as clearance seal machining tolerances). The Philips Stirling cycle model was used to develop an optimal design meeting all the design criteria.

Since launch conditions are the primary new considerations in this second generation design, a description of the various vibration analyses is provided in the next section. Other component level improvements such as new reluctance radial position sensors with excellent temperature stability, and an integrally formed aluminum/titanium cold end heat exchanger are described following the vibration section. Finally, primary system design parameters and predicted performance levels are presented in the last section.

3. Vibration considerations

The Engineering Model refrigerator demonstrated the concept of using magnetic bearings and linear drive methods to obtain long-life operation. The Prototype refrigerator described in this paper will demonstrate these concepts in actual space-qualified hardware. As part of this effort, the refrigerator dynamics were modelled to determine the effect of launch vibrations and the design was tailored to achieve an acceptable system response.

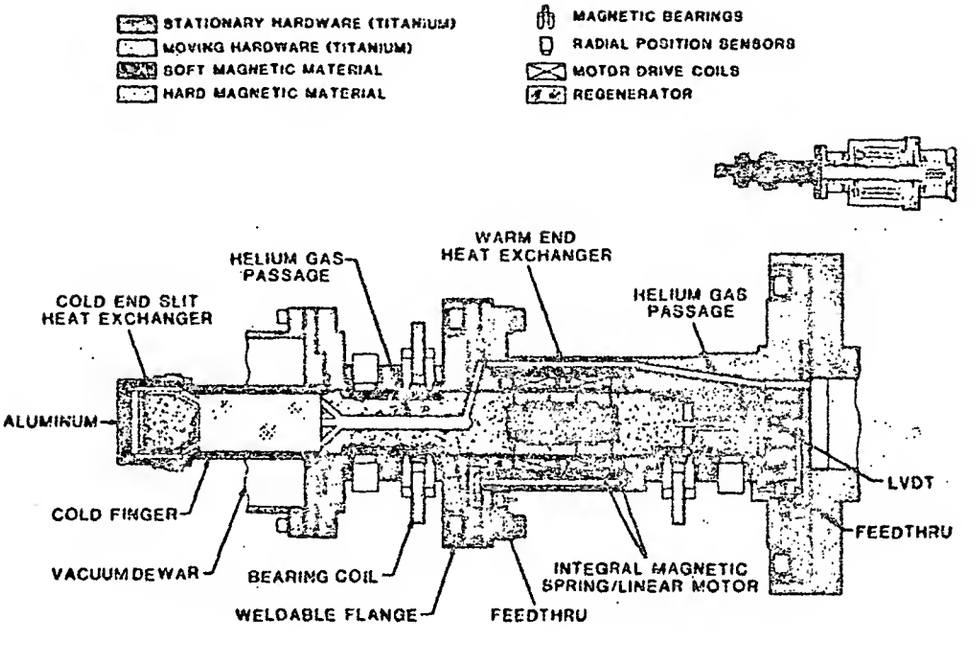

a.

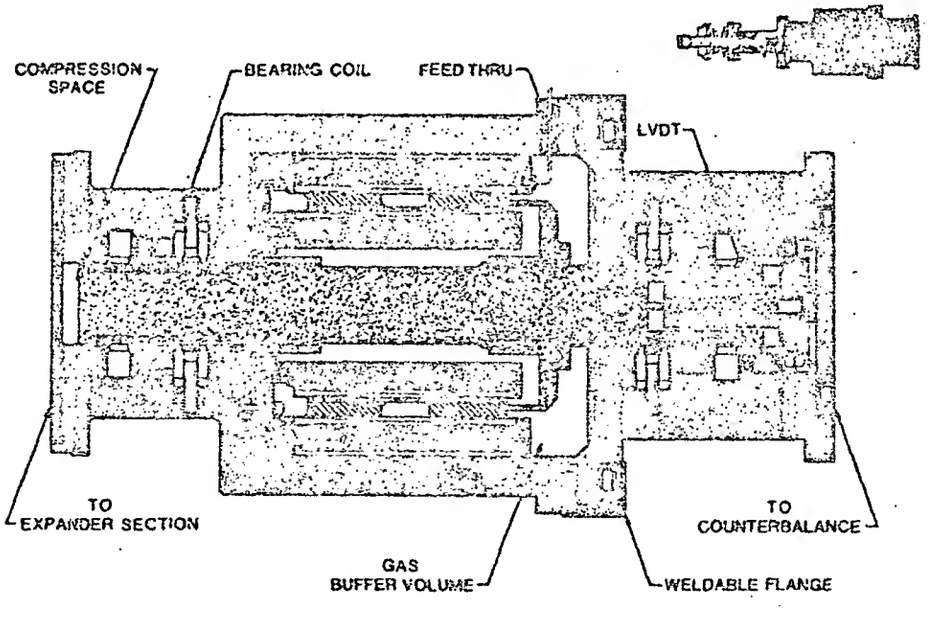

b.

Figure 1. Refrigerator sectional lay-outs
a. Expander (displacer) section
b. Compressor (piston) section

3.1 Refrigerator dynamics

The contiguous surfaces in the clearance seals are the area most susceptible to vibrational damage. If the ultra-clean titanium surfaces of the clearance seals come in contact, potentially catastrophic failure in the form of galling is possible. Magnetic bearings accurately center the shafts within the bores thus maintaining the non-contact operation of the clearance seals. The vibration analyses are focused on determining the bearing performance required to maintain non-contact support during launch. The launch vibrations are described by three independent specifications; random, acoustic, and quasi-static. The analyses for each of these excitations follow.

The bearing performance requirements can be determined from the solid-body vibration amplitudes of the refrigerator. For this purpose, simple first and second order models are sufficient. Forces are transmitted to the refrigerator through the isolation mount (fig. 2) and by acoustic coupling directly to the housing. The vibration amplitudes are calculated assuming a lumped spring-mass system model (fig. 3).

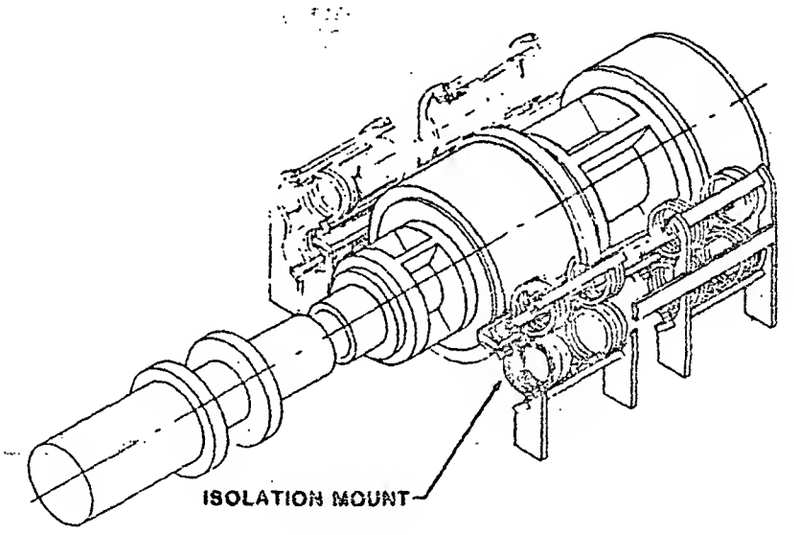

Figure 2. Refrigerator isolation spring mount design

The random vibration specification is a power spectral density (PSD) function describing the random vibrations of the shuttle mount surface. PSD is a statistical method of describing the frequency content of random signals. The vibration amplitude PSD is determined via the given acceleration PSD and the calculated inertial transfer function. The random vibration specifications and the resulting refrigerator vibration PSD function are shown in figure 4. The mounting surface vibrations are effectively filtered by the 7.0 Hz isolation spring mount. The resulting solid-body RMS vibration amplitude is 17 μm with most of the vibration energy contained below 45 Hz.

Acoustic sound energy also induces vibrations in the refrigerator. The pressure difference across the refrigerator produces a net force on the housing. In general, the force on a cylinder perpendicular to a 2-D pressure field is

$$F = A \int_0^{2\pi} P(\theta) \cos(\theta)\, d\theta \qquad (1)$$

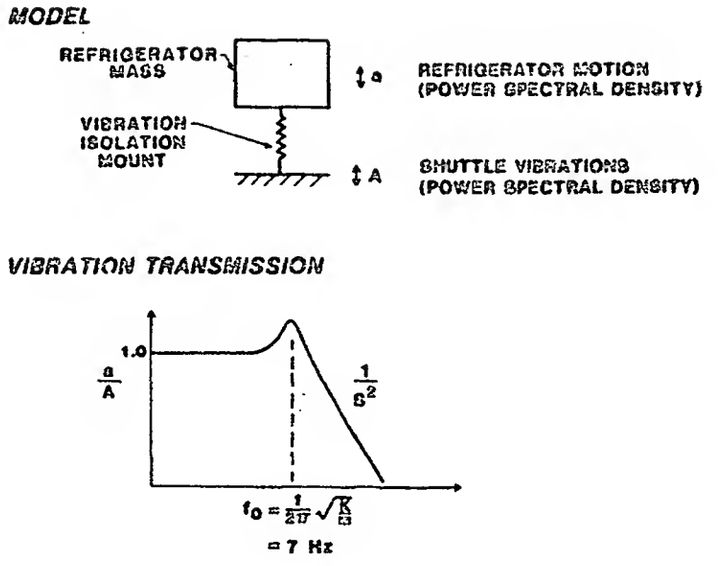

Figure 3. Random vibration lumped spring-mass system model

where A is the cylinder radius and $P(\theta)$ is the pressure distribution over the cylinder surface. Assuming a sinusoidal plane wave, the peak force is

$$\hat{F} = \frac{2 P_0 c}{\omega E} \tag{2}$$

where P_0 is the peak pressure, ω is the angular frequency of the pressure wave, c is the speed of sound in air and E is defined to be

$$E = \frac{1}{2} \left\{ J_0^2(ka) + J_2^2(ka) + Y_0^2(ka) + Y_2^2(ka) - J_0(ka)J_2(ka) - Y_0(ka)\, Y_2(ka) \right\}^{\frac{1}{2}} \tag{3}$$

where $k = 2\pi/\lambda$ and J and Y represent the Bessel functions of the first and second kind respectively.

The acoustic coupling is maximum when the housing diameter is 40% of the sound wavelength. The coupling decreases monotonically at higher and lower acoustic frequencies. Using this model and the acoustic sound pressure specifications shown in figure 5, the refrigerator RMS vibration amplitudes are determined to be less than 2.0 μm. The vibration energy is centered at 40 Hz and is negligible above 100 Hz.

NASA utilizes a third specification to include the effects of shock loads, mount amplification, and launch uncertainty. This specification is termed "Quasi-Static Loading" and is by far the most severe of the three specifications on the refrigerator design. This data was compiled from previous flights and represents the maximum acceleration levels measured on devices with similar isolation mounts.

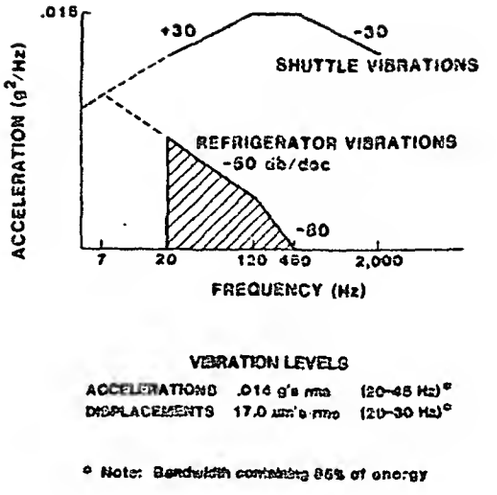

Figure 4. Space shuttle random launch vibrations: specifications and refrigerator vibrations

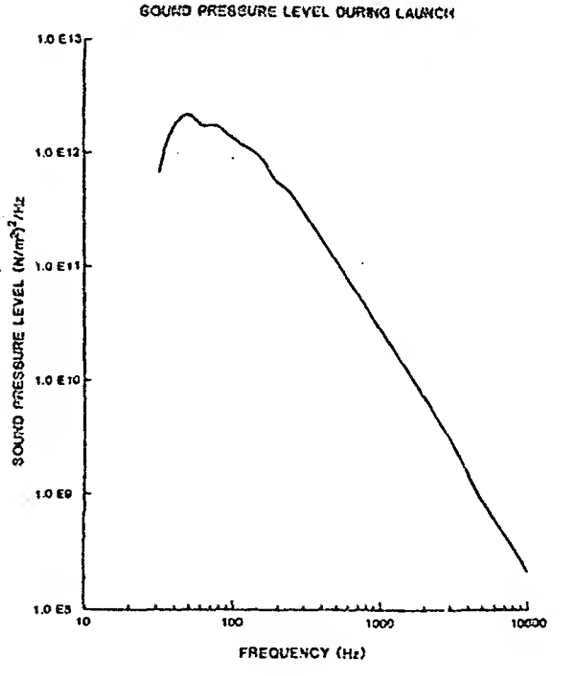

Figure 5. Sound pressure level during launch

The specification describes the vibrations during the three launch phases: lift-off, transonic/maximum aerodynamic pressure, and ascent. Each phase has an ac and dc acceleration component which is applied to the refrigerator simultaneously in three orthogonal axis for a specified duration. The isolation mount frequency determines the ac acceleration specifications; the design frequency of 7.0 Hz yields the specifications presented in table 1.

Table 1. Quasi-static launch vibrations

Occurrence	D.C. Acceleration (g's)	A.C. Acceleration at 7.0 Hz (g's)	Vibration Duration (seconds)
Lift-off	1.5	5.4	20.
Transonic/Maximum Aerodynamic Pressure	3.0	2.7	10.
Ascent	3.2	0.	100.

Meeting these specifications requires either improvements in the magnetic suspension system to totally prevent contact or changes to the titanium surfaces to permit limited contact during launch. The following design changes improve the suspension system performance. In addition, surface treatments will improve the clearance seals to permit limited contact during launch.

3.2 Design changes

The Engineering Model magnetic bearing stiffness must be improved 60-70 dB to avoid contact during launch. The magnetic bearings are controlled by a closed-loop control system which monitors the shaft position and excites the appropriate electromagnets to center the shaft. The achievable open-loop gain of the control system, which determines the apparent bearing stiffness, is limited by the shaft dynamics. The 70 dB gain improvement was demonstrated in a test fixture with a solid (rigid) shaft. Thus, if the shaft dynamics can be improved sufficiently, the refrigerator will withstand the launch vibrations.

The design changes made to improve the shaft dynamics are presented in table 2. The goal is to increase any resonant frequencies beyond the desired control bandwidth and to increase the system damping. The increase in diameters, shorter lengths, and decreased suspended mass all increase the resonant frequencies. The system damping is improved by decreasing the radial clearance in the clearance seal. This cylindrical annulus is filled with the working gas and acts as a viscous dashpot as the shaft moves radially. Decreasing the clearance 25% will double the damping forces. These changes result in the dynamics presented in table 3. These improvements are sufficient to achieve the required bearing stiffness.

Table 2. Design changes to improve shaft dynamics

	Engineering Model	Prototype
• Increase stiffness		
Displacer diameter (cm)	2.0	3.16
Piston diameter (cm)	3.68	4.45
Cold finger diameter (cm)	2.15	3.31
Piston wall thickness (cm)	0.26	0.57
• Increase damping		
Clearance seal gap (μm)	25.	17.
Clearance seal length (cm)		
Piston	4.0	8.0
Displacer	2.5	5.0
• Minimize cold finger suspended mass		
Heat exchanger material	Copper	Aluminum

Table 3. Improved shaft dynamics

	Engineering Model	Prototype
• Squeeze film damping breakpoint (kHz)		
Piston	2.5	50-85
Displacer	0.7	45-155
• First bending resonances (Hz)		
Piston	400	900
Displacer	840	1800

The clearance seal surfaces will be treated with titanium nitride to improve the wear properties. This provides additional protection to the clearance seals and minimizes the chance of catastrophic failure should the surfaces come in contact during launch. Various surface treatments were investigated. Clearance seal samples were coated and subjected to the launch vibrations. The surfaces were analysed microscopically. The samples were subjected to increased vibration amplitudes until excessive wear occurred. The treatments tested and the relative performance data are presented in table 4.

Table 4. Surface treatment evaluation results

Shaft Number	Surface Treatment	Acceleration level (g's) A.C.	D.C.	Results
0	none	3	5	Severe fretting & abrasion
1	TiN plated	3	5	No degradation
1	TiN plated	10	25	Fretting
2	Sn-N implanted	3	5	Minor fretting
2	Sn-N implanted	6	10	Extensive fretting
3	Ag-N vs C implanting	3	5	Light fretting
4	Ti-N plated	3	5	Light abrasion
4	Ti-N plated	6	10	Light abrasion
4	Ti-N plated	9	15	Severe abrasion
5	C implanted	3	5	Moderate fretting
6	C implanted	3	5	Moderate fretting

4. Component improvements

In addition to the work discussed above, several key system components have been improved vis-a-vis the Engineering Model design. Improvements in long term temperature stability and reliability of the bearing control system result from replacing the eddy current sensors in the Engineering Model with ferrite reluctance position sensors. An aluminum slit heat exchanger is used to reduce the cantilevered mass at the end of the cold finger. System efficiency is improved with a magnetic spring integrated in the displacer linear motor and by using a novel low frequency switching driver for the piston motor. Although the thermodynamic efficiency is reduced from the Engineering Model, the overall efficiency (the ratio of cooling to electric input power) has increased as a result of the improved drive systems. Detailed descriptions of each of these improvements follow.

4.1 Aluminum cold end heat exchanger

The Engineering Model refrigerator has a copper annulus cold end heat exchanger. The Flight Prototype uses a slit aluminum heat exchanger. The slits provide an equivalent heat transfer surface area with a shorter heat exchanger length. A reduction in weight results from the reduced material density. The fabrication of the aluminum heat exchanger is outlined in figure 6 [3].

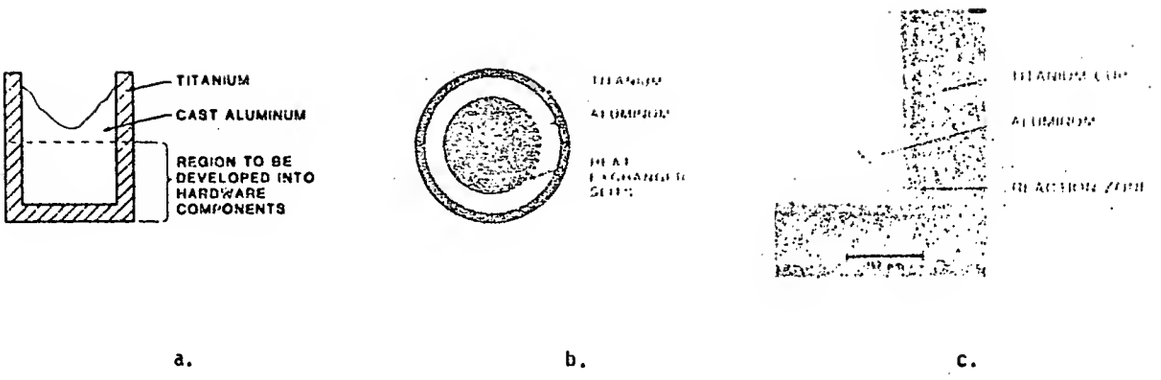

a. b. c.

Figure 6. a. Aluminum-titanium heat exchanger fabrication
b. Heat exchanger photograph
c. SEM photographs of bond interface

A 5 Al-2.5 Sn titanium cup and a mating commercially pure aluminum piece are cleaned and degassed. The assembly is heated in a high vacuum furnace. As the aluminum melts, it wets and adheres to the titanium surface forming a metallurgical joint. The bonded structure is then hipped to remove any voids and improve the structural properties. The center of the aluminum material is removed to form a thick walled composite structure. The heat exchanger slits are electro-discharged-machined (EDM) in the aluminum walls. The outer titanium wall provides the needed strength for pressure vessel containment and is subsequently welded to the cold finger.

A heat exchanger sample has been temperature cycled 1000 times from room temperature to 77 Kelvin and 10 times to 4.2 Kelvin. Metallographic and scanning electron microscopy of the tested sample show good metallurgical bonding. Tensile tests of a cast sample showed that the bond strength exceeds the strength of the aluminum. Figure 6c is a photograph of the aluminum/titanium joint indicative of a superior bond. A heat exchanger sample pressurized to four times the design pressure is currently being cycled from room temperature to 77 Kelvin. To date, 1,000 cycles have been accumulated with no indication of failure.

4.2 Integral magnetic spring/linear motor

During operation, the displacer shuttles gas between the cold and warm ends. The displacer reciprocates at a specified frequency, stroke, and phase relative to the piston motion. The displacer construction includes the regenerator mesh, bearing armature and radial position 'target' material, structural walls, and linear motor. For designs of this type, the fluid damping forces acting on the displacer are small in comparison to inertial forces during operation. Ideally, for compact cooler design, the machine should operate at the highest frequency allowed by the regenerator heat capacity and fluid viscous losses. In addition to the size and weight reduction, the linear compressor motor size decreases with higher speeds, since the output force decreases. However, the displacer motor power loss is proportional to the fourth power of frequency while the cooling capacity is only linearly proportional to frequency. The significance of the displacer motor power has resulted in larger, lower frequency cooler designs.

Due to the large ratio of inertial to damping forces, a resonant displacer/spring system would greatly reduce the required motor power. In fact, 'free displacer' coolers have been made which have no displacer motors. These coolers use the operating pressure wave to drive a resonant displacer/mechanical spring system.

Long life mechanical springs can be designed provided the operating stress levels are sufficiently low. The damping forces for a well mounted mechanical spring are also quite low. However, experience with mechanical spring balancers has shown that small particles are generated during operation. These particles would be catastrophic to the clearance seals. Thus, mechanical

springs could not be used in the design. Gas springs have no wear problems, but do have limited linearity, higher damping than mechanical springs, and do require an additional clearance seal. For these reasons, the gas spring was also not used in this design. Magnetic springs, on the other hand, do not need clearance seals and have no life-limiting properties. As a result of the advances made in permanent magnet material, new, high strength magnets with minimal long term aging and good temperature stability are now available. These improvements have made magnetic springs feasible and the Flight Prototype incorporates one in the displacer design.

One advantage of the Engineering Model's linear motor drive system is the freedom to adjust the displacer and piston strokes independently as well as the phase. In a free displacer design, control and flexibility is lost though fewer components are needed. Thus an adjustable spring or a spring and motor is desirable to maintain operating flexibility.

The Flight Prototype incorporates such an integrated magnetic spring/motor. The motor provides control of the displacer motion. A schematic of the integral spring/motor with the displacer at full stroke is shown in figure 7. The moving magnets act as springs and interact with the stationary coil to produce a force which is proportional to the current in the coils.

The construction of the motor is very similar to the displacer linear motor of the Engineering Model. Radially magnetized magnets are added to the stator at both ends of the coils to provide a self-centering magnetic spring. Good linearity is achieved over the design stroke through proper positioning of the concentric magnets. Another advantage in this design is the single diameter construction. No dead space or void volumes are introduced which would have existed with a conventional face-to-face repulsion magnet spring. The springs reduce the peak force requirements of the motor. Table 5 compares the power requirements of the integral spring/motor design to a conventional linear motor design with equivalent size envelopes. In both cases SmCO5 magnets are used because of their very rigid magnetization and excellent thermal and long term aging stability.

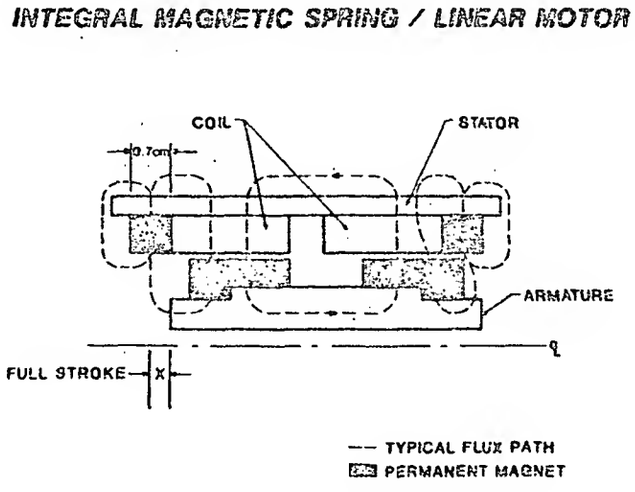

Figure 7. Schematic of integral displacer magnetic spring/linear motor.

Table 5. Power comparison: Integral spring/motor vs. linear motor

	Spring/motor	Conven. linear motor
Peak motor force (N)	12	46
Magnet moving mass (Kg)	.033	.035
Total electric power (W)	5	20

Eddy current damping generated in this magnetic spring is difficult to accurately predict. These eddy currents dissipate stored energy and lower the spring quality factor (Q). Another problem with a magnetic spring of this design is the radial instability and resulting side loads. These side loads occur not only from magnetic eccentricities resulting from mechanical construction, but also from magnet non-uniformity. These side loads have static as well as dynamic components. Because of the difficulty in estimating these effects, tests were performed with a dedicated test fixture.

4.2.1 Static spring test results

Axial springs of this design have a radial instability stiffness which is less than or equal to negative one half the axial stiffness[4,5]. The sign is critical since a 10 N/m axial stiffness PM spring has a radial stiffness ranging from negative 5 N/m to negative infinity. For designs involving no soft magnetic material the inequality qualifier can be removed.

The stiffness of a simple magnet pair (no soft magnetic material) was tested and compared to a finite element analysis of the same geometry (fig. 8). The characteristic geometry of the magnet rings is very close to the spring/motor design. Side load tests were performed by displacing the inner ring toward the outer ring and measuring the radial force. The radial stiffness was measured to be negative one half the axial stiffness. The side loads for zero mechanical eccentricity of various magnet pairs were measured to determine the magnet non-uniformity. Table 6 summarizes the test results. These results indicate that matched magnet segments must be used to produce acceptable performance.

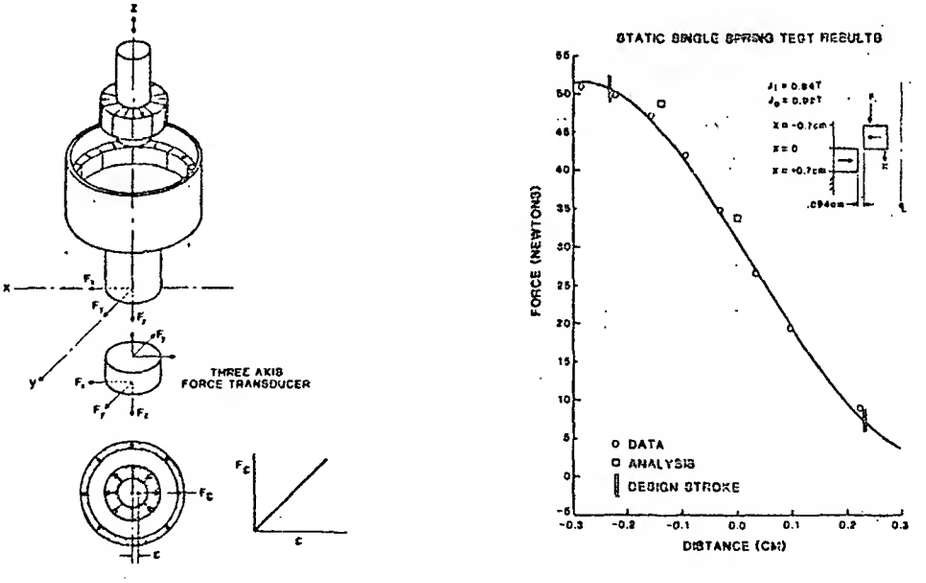

a. b.

Figure 8. Static test of single magnet pair vs. analysis
a. Test set-up
b. Axial test results

Table 6. Static side load test results

Radial instability of single magnetic spring pair

Axial stiffness at mid position	11,000 N/m
Radial instability stiffness	
Theoretical analysis	5,500 N/m
Finite element analysis	5,500 N/m
Measured	5,000 - 7,000 N/m

Magnet non-uniformity

Magnet pair number	1	2	3	4
Peak radial side force (N) (in concentric position)	2.0	1.1	2.6	0.25
Equivalent geometric (cm) eccentricity			0.047	0.005

4.2.2 Dynamic test results

Following these static tests, two sets of springs were mounted to an active radial magnetic bearing test fixture which exhibits no friction and extremely low damping in the axial direction. Figure 9a is a schematic of the test fixture. The integral magnetic spring/motor was in effect split and placed at either end of the bearing test fixture. Figure 9b is a scope trace of the position of the moving mass vs. time resulting from an initial step displacement. The resulting Q of about 70 indicates that there is very little eddy current damping in the magnets. The quality factor, Q, does get lower as additional magnets or magnetic material is placed near the spring indicating that eddy current damping is not negligible.

The test set-up was further modified to test the integral motor/spring concept. An additional small magnet ring was attached to each inner magnet ring as in figure 9c. A coil is placed around each inner magnet ring. This test was performed to verify the analytic procedure used to determine the force constant of the displacer motor. Both dc and ac tests were performed using the motor to excite the moving mass. The dc force constant of the motor agrees well with the predictions. The displacer is driven off-resonance (as it will be in operation) and open-loop and the resulting frequency spectrum of the displacement is recorded. Figure 9d(1) is a force displacement curve of the spring for positive and negative displacements. At low amplitudes, the curves match well, indicating that there should not be any even harmonics in the displacement spectrum. At larger strokes, the curves vary indicating that even harmonics will be present. The resulting frequency spectrum measurement of the displacement is shown in figure 9d(2). These harmonics produce insignificant adverse effects on the thermodynamics.

Through the introduction of bonded high energy product magnets, the damping can be further reduced because of their very high resistivity. In a free displacer design, the motor can be eliminated and axially magnetized springs can be used thus simplifying the fabrication.

4.3 Radial position sensors

The accuracy of the radial position sensors in a magnetic bearing system determines the limit of the achievable accuracy of that system. The Engineering Model cooler which employed magnetic bearings, used eddy current sensors as the means of measuring radial position. These sensors, however, are not without drawbacks: they must be isolated from the helium working gas by a ceramic window and titanium pressure wall, and their extreme temperature drift precludes the use of these sensors in the single-ended mode. Thus, each axis requires two matched sensors, two window assemblies which tend to trap particulates, and high frequency differential electronics to acquire a single position signal (fig. 10).

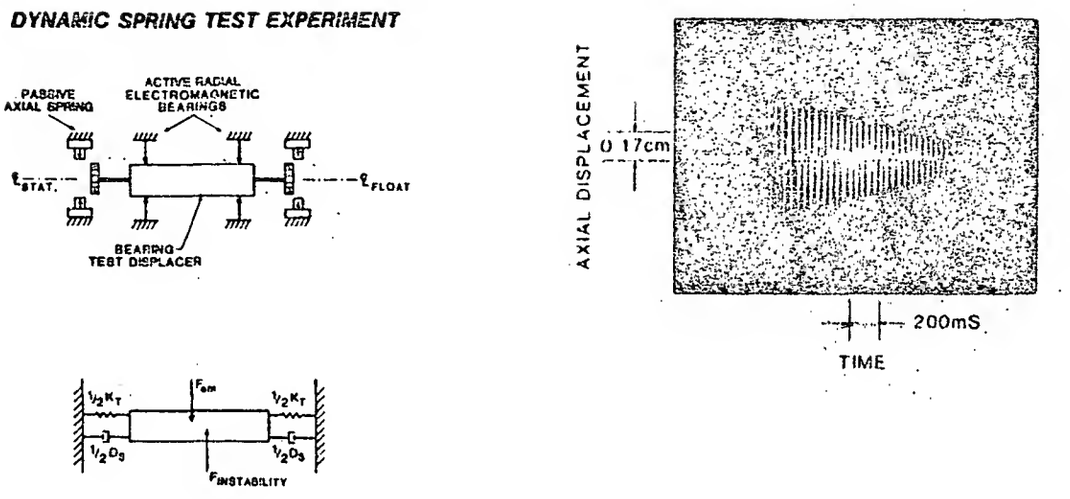

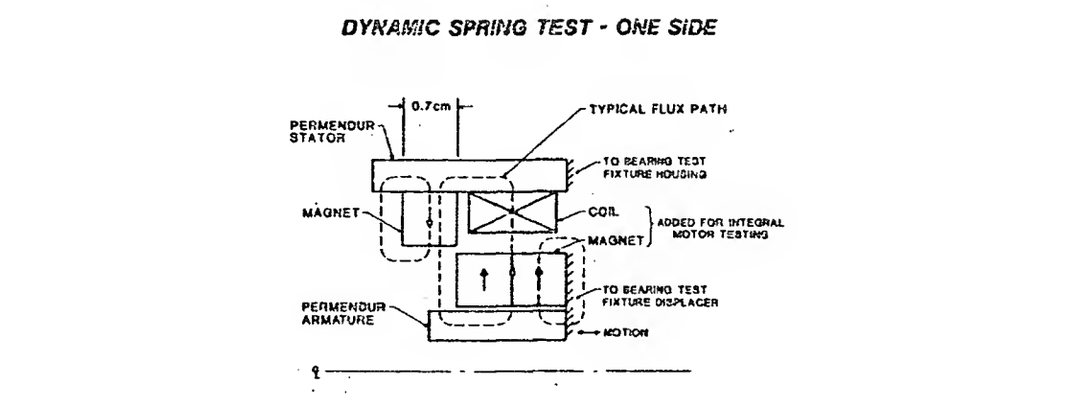

Figure 9. Dynamic test results
a. Dynamic test schematic
b. Damping with permendur backing (Q = 70)
c. Dynamic test fixture with coil and additional magnets
d. Motor test results - displacement spectrum (see next page)

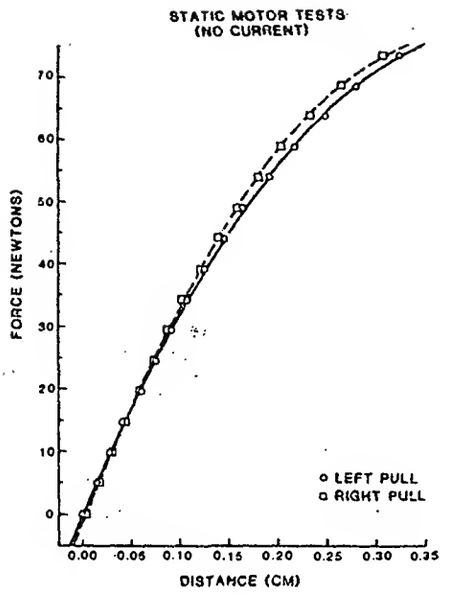

d(1) pull to left and right

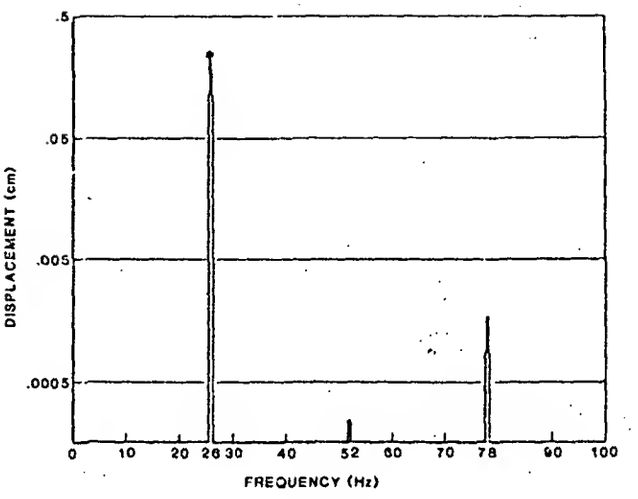

d(2) large stroke

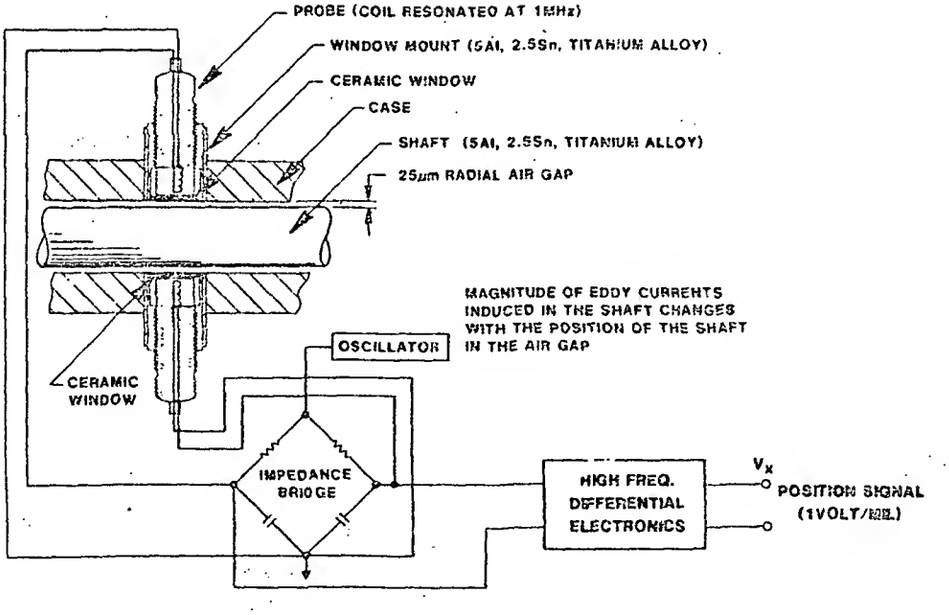

Figure 10. Differential eddy-current sensors

In an effort to simplify both the mechanical and electrical aspects of the radial position sensing, a number of alternative sensing schemes were considered. The major features desired for the new radial position sensor are summarized below:

- Single-ended (to allow redundancy)
- High bandwidth
- Negligible temperature drift
- High signal-to-noise ratio
- Simple electronics (reliability)
- Repeatable, stable, easily cleaned, mechanical assembly

The most promising method, with regard to simplicity of electronics, was that of variable reluctance sensing. Furthermore, with the application of ferrite to a reluctance sensor, eddy currents are eliminated; and thus, high bandwidth is achieved. With appropriate magnetic and electronic design, a reluctance sensor also offers a reasonably linear response with negligible temperature drift in a single-ended configuration. Finally, the reluctance sensor greatly improves the mechanical design if the ferrite sensor itself can penetrate the titanium wall, be ground flush with the wall, and serve as a hermetic barrier. This mechanical design required a hermetic ferrite/ceramic/titanium joint which was the subject of a major effort in materials technology. A functionally representative schematic of the ferrite sensor is shown in figure 11.

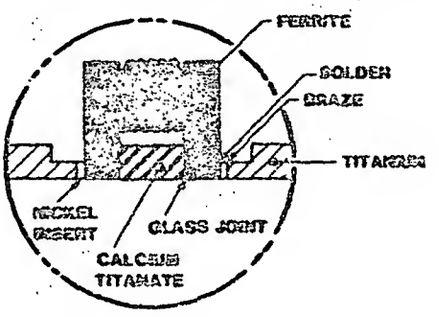

Figure 11. Ferrite radial position sensor

Extensive testing of the ferrite sensor was performed to measure the position sensitivity and the temperature drift in the single-ended mode. Inductance measurements were taken at constant temperature over the range of 0 - 4 mils (fig. 12). The data shows that the inductance, L, is

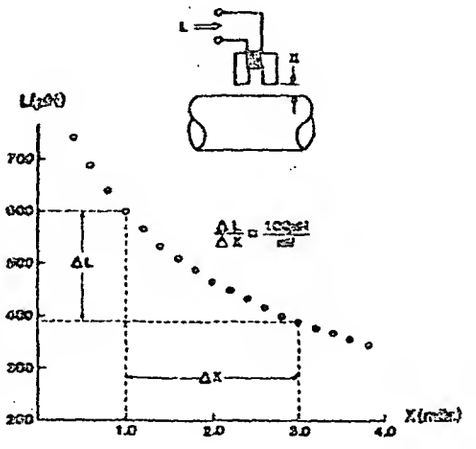

Figure 12. Inductance L vs. position x

inversely proportional to the gap size, x, with a sensitivity, dL/dx, of approximately 100 μH per mil. This represents a change in impedance of 20% per mil of displacement for the ferrite sensor as compared to roughly a 1% change in impedance for existing eddy current sensors.

The relatively high sensitivity to position was one major step towards the minimization of temperature drift; the next criterion to consider was the sensitivity of inductance to temperature.

The temperature sensitivity is measured using a specially designed test fixture which maintains a fixed gap between sensor and target. The fixture is placed in a temperature controlled oven which is cycled from 20 °C to 80 °C repeatedly. The inductance of the sensor is continuously monitored and recorded to quantify any drift in inductance due to a change in temperature.

Figure 13 is a plot of inductance vs. temperature for a fixed 3 mil gap over the range of 20 - 80 °C. The data shows an increase in inductance with temperature from 390 μH at 20 °C to 395 μH at 80 °C. This 5 μH change in inductance translates to a position error of approximately 50 u-inches which represents only 5% of the 1 mil radial clearance between the piston and cylinder.

Previously, the acceptance criterion for matching eddy current probes was expressed in terms of a maximum position error of 200 u-inches or 20% of the 1 mil radial clearance with the probes used in the differential mode. Thus, the ferrite radial position sensor offers much improved temperature stability with the added advantage of operating in the single-ended mode.

Having achieved adequate temperature stability through appropriate choice of materials and geometrical design, the linearity and sensitivity of the electronics was tested. The output voltage as a function of gap size is plotted in figure 14 along with a line describing the ideal linear output.

The close fit of data points to the ideal curve shows a fairly linear relationship between output voltage and position, and a sensitivity of about 10 volts per mil.

In summary, the ferrite radial position sensor has exhibited excellent performance over a wide temperature range. It has demonstrated adequate linearity, good sensitivity, and exceptional temperature stability, while obviating the need for differential sensing and facilitating the incorporation of redundant sensing techniques. Furthermore, it has greatly simplified the electronics design which leads to a lower parts count and, hence, increased reliability. And finally, the mechanical assembly provides a flush bore which is hermetic and can be easily cleaned.

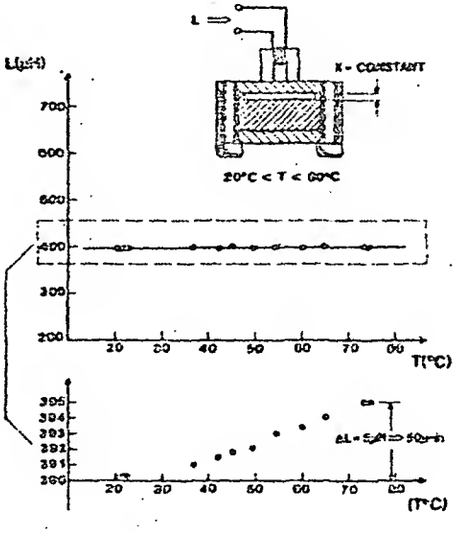

Figure 13. Inductance vs. temperature

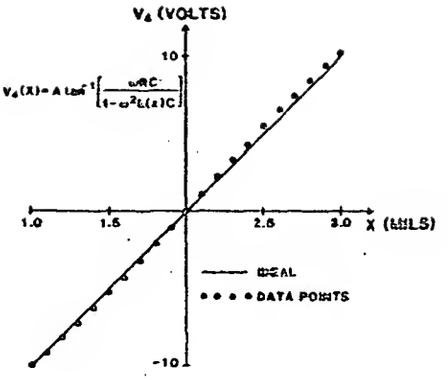

Figure 14. Output voltage (V4) vs. position (x)

4.4 Synchronous linear motor controller

In the Engineering Model cooler, moving magnet linear motors are used in axial control loops to prescribe the reciprocating motions (i.e. amplitude, phase, speed & center position) of the piston and displacer. The axial control is performed with position servo loops employing LVDTs to measure position and linear amplifiers to drive the motors. The linear amplifiers exhibit excellent reliability and high bandwidth, and in general meet all the performance requirements of the original design specifications. However, the poor (~40%) efficiency of the linear drivers precludes their use in a spaceborne system. Therefore, alternative driving methods were investigated, specifically, switching drivers which would provide an axial control system with high reliability and maximum efficiency.

High frequency (100 kHz) switching amplifiers have been used for this application and have achieved efficiencies on the order of 75% with a bandwidth of 1 kHz. Using this type of amplifier, one could directly replace the linear amplifier and use the same control system. However, for high current applications, viz. the piston driver, the high frequency switcher becomes complex and less reliable due to parasitic oscillations associated with the paralleling of power MOSFET transistors and the finite reverse recovery times associated with high current diodes.

A significantly different approach to the axial control provides an alternative driving scheme. Using a nonlinear control system which employs phase lock loop techniques and takes advantage of the electro-mechanical filtering properties of the linear motors. The amplifier used in this system produces a switching waveform at the same frequency as the refrigerator operating frequency. The ac component, the dc component, and the phase of the waveform are controlled by three separate inputs to the amplifier as shown in figure 15.

The amplitude of the fundamental component of the switching waveform is varied by a common mode modulation of the positive and negative pulse widths. The dc component of the waveform is varied by a differential modulation of the positive and negative pulse widths; and the phase and frequency of the switching waveform are prescribed by an ac signal at the third input to the amplifier. These three control lines are used in three distinct control loops to accurately prescribe the amplitude, center position, and phase of a piston or displacer motor (fig. 16).

In the first control loop, a low-pass averaging circuit is used to feedback the dc position of the motor and compare it to a reference signal; the resultant error signal is then compensated and used to adjust the dc component of V_{out} to achieve the desired dc position. A second control loop is realized by using a peak to peak detector to determine the stroke of the reciprocating motor. The stroke amplitude is compared to a reference signal, and the resultant error signal is compensated and used to adjust the ac component of V_{out} to achieve the desired stroke of the motor. Finally, a third control loop is formed to control the phase of the motor.

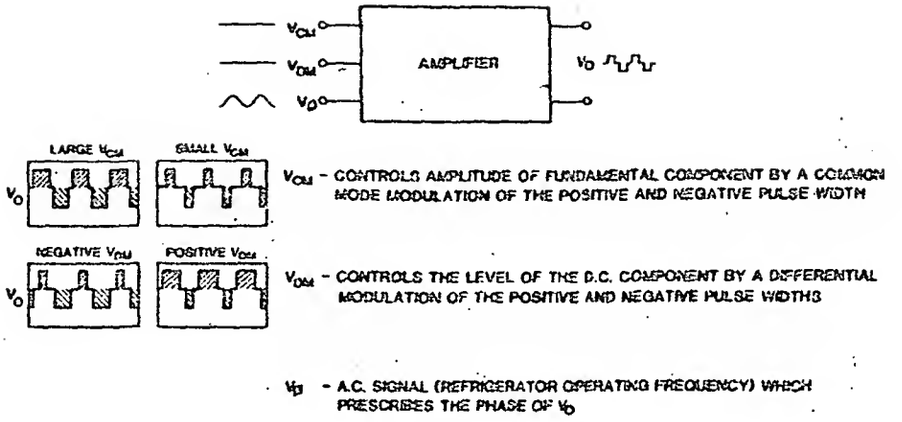

Figure 15. Open loop amplifier

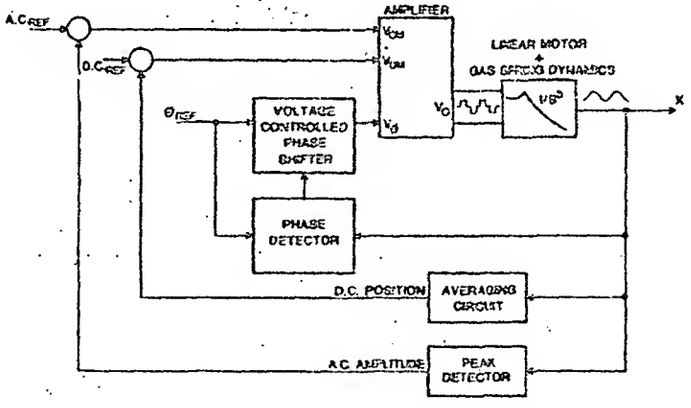

Figure 16. Control scheme showing 3 distinct control loops

A clock signal provides the frequency and phase reference onto which the motor phase is locked via phase locked loop techniques.

A prototype system which can deliver 500 watts of real power to the piston motor with an amplifier efficiency of 95% was designed and fabricated. The system exhibits excellent control of critical operating parameters with negligible distortion of the desired sinusoidal motion (fig. 17) and a surprising tolerance to noise and non-ideal sensor performance.

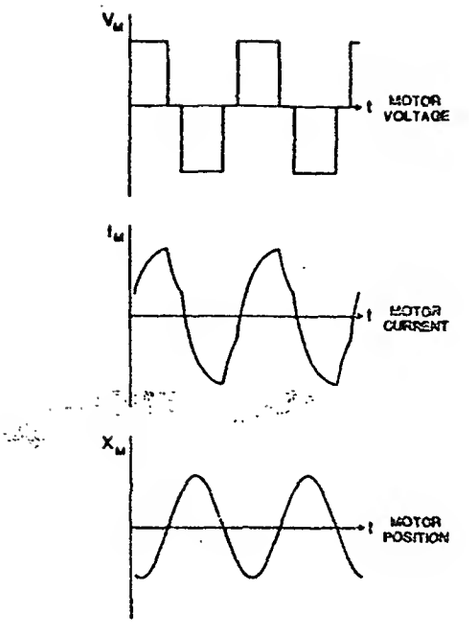

Figure 17. Characteristic waveforms: Voltage, Current, and Position

Since the switching frequency of the amplifier is very low, i.e. the same as the operating frequency of the refrigerator (15 - 25 Hz), the design of the amplifier is greatly simplified, resulting in a lower parts count and hence higher reliability. Furthermore, at these frequencies, switching losses are negligible, and transistors are easily paralleled to achieve very high efficiencies.

In summary, the synchronous motor controller, although exhibiting a slower transient response, provides better efficiency, potentially greater reliability, and better control of steady-state operating parameters than is possible with either a linear amplifier or a high frequency switching amplifier used in a classical position servo loop.

5. System performance

Table 7 is a summary of the key design parameters of the Flight Prototype model. System performance is summarized in Table 8. The thermodynamic efficiency of the design is comparable to the Engineering Model. Overall reduction in system power results from higher efficiency driver systems and the inclusion of the magnetic spring in the displacer motor. The counterbalance design (including power requirements) have not yet been addressed.

Table 7. Flight prototype design parameters

Piston design stroke (mm)	7.4
Piston diameter (cm)	4.45
Displacer design stroke (mm)	2.3
Displacer diameter (cm)	3.155
Operating speed (Hz)	18.9
Charge pressure (N/m^2)	1.69 E6
Regenerator wall thickness (mm)	0.5
Cold finger wall thickness (mm)	0.5
Displacer moving mass (Kg)	0.9
Piston moving mass (Kg)	3.95
Clearance seal gap (μm)	17

Table 7. Flight prototype design parameters (cont.)

Regenerator:	
Material	phosphor bronze
Cross sectional area (cm^2)	7.31
Length (cm)	6.0
Wire diameter (μm)	53.
Fill factor	0.36
Piston motor:	
Motor type	moving magnet linear motor
Yoke material	4% SiFe
Magnet material	SmCo5, BH max = 23 MGOe
Peak motor force (N)	220
Mechanical output power (W)	100
Efficiency (%)	75
I^2R Loss (W)	30

Table 8. Flight prototype system performance

Design cold production (W)	5.
Cold end temperature (K)	65.
Warm end temperature (K)	300.
Thermodynamic shaft input power (W)	100.
Piston motor input power (W)	135.
Displacer motor input power (W)	5.
Total input power to motors (W)	140.

6. Summary

A second generation magnetically suspended, linear Stirling cycle cryogenic refrigerator has been designed to meet the space shuttle launch requirements. The design changes are primarily focused on improving the refrigerator dynamics and thus its capability to withstand the launch vibrations. These include; increased structural resonant frequencies, increased ac/dc bearing force capability, and increased gas film damping. Other improvements, which increase system reliability and efficiency, include an integral displacer magnetic spring/motor, ferrite variable reluctance position sensors, surface treated clearance seals, and an aluminum/titanium cold-end heat exchanger. The work summarized in this paper is being supported by the NASA-Goddard Space Flight Center. (Contract Number NAS5-25688).

References

[1] Philips Laboratories, division of North American Philips Corp., Design and Fabrication of a Long-Life Stirling Cycle Cooler for Space Applications, Phase I and II - Engineering Model, Final Report: Sept. 1978 - Dec. 1982, F. Stolfi, et al, NASA Contract NAS5-25172, Briarcliff Manor, NY, March 1983.

[2] Philips Laboratories, division of North American Philips Corp., Parametric Testing of a Linearly Driven Stirling Cryogenic Refrigerator, F. Stolfi and A. Daniels, 3rd Cryocooler Conference on Refrigeration for Cryogenic Sensors and Electronic Systems; Boulder, CO, Sept. 1984.

[3] Novel Titanium-Aluminum Joints for Cryogenic Cold Finger Structures, H.M. Meehand and R.C. Sweet, Advances in Cryogenic Engineering, Vol 27, Plenum Press, New York, 1981.

[4] Directivity and Stability of Coaxial Permanent Magnet Systems, Th. Gast, A. Mirahmadi and F.E. Wagner, Paper no. V-2 at 5th International Workshop on Rare Earth-Cobalt Permanent Magnets and Their Applications; Roanoke, VA, June 1981. (Book by University of Dayton, KL-365, Dayton, Ohio 45469, USA).

[5] Permanent Magnet Bearings and Couplings, Jean-Paul Yonnet, IEEE Transactions on Magnetics, Vol. MAG-17, No. 1, January 1981, pp 1169-1173.